Scatter correction algorithm without extra exposure for dual-energy digital mammography

Xi Chen[1], Xuanqin Mou[1], Hao Yan[1], Hengyong Yu[2], and Lei Zhang[3]
[1]Institute of Image Processing & Pattern Recognition, Xi'an Jiaotong University, Xi'an, Shaanxi, 710049, China
[2]Biomedical Imaging Division, School of Biomedical Engineering and Science, Virginia Tech., Blacksburg, VA, 240601, USA
[3]Department of Computing, Hong Kong Polytechnic University, Hung Hom, Kowloon, Hong Kong

ABSTRACT

X-ray scatter leads to erroneous calculations of dual-energy digital mammography (DEDM). The existing methods for scatter correction in DEDM are using anti-scatter grids or the pinhole-array interpolation method which is complicated and impractical. In this paper, a scatter correction algorithm for DEDM is developed based on the knowledge that scatter radiation in mammograms varies slowly and most pixels in mammograms are non-microcalcification pixels. The proposed algorithm only uses the information of low-energy (LE) and high-energy (HE) images. And it doesn't need anti-scatter grids, lead sheet and extra exposures. Our results show that the proposed scatter correction algorithm is effective. When using the simple least-squares fit and linear interpolation, the scatter to primary ratio (SPR) can be decreased from ~33.4% to ~2.8% for LE image and from ~26.2% to ~0.8% for HE image. Applying scatter correction to LE and HE images, the resultant background signal in the DE (dual-energy) calcification image can be reduced significantly.

Keywords: dual energy, mammography, scatter correction

1. INTRODUCTION

Breast cancer is a major health concern for women. Microcalcifications (μCs) in mammograms, the often earliest signs of breast cancer, can be obscured by overlapping fibroglandular tissue [1]. Dual-energy digital mammography (DEDM) is considered as a promising technique to improve the detection precision of μCs. In DEDM, high-energy (HE) and low-energy (LE) images of a breast are acquired using two different x-ray spectra. By exploiting the difference in x-ray attenuation between different materials at different x-ray energies, the HE and LE images can be synthesized to suppress the contrast between adipose and glandular tissues and subsequently generate the dual-energy (DE) calcification image.

One important concern for DEDM imaging is the scatter radiation arising from the x-ray beam. In Cooper's experiment, the measured scatter-to-primary ratios (SPRs) at 28 kVp for 4 cm breast phantom were 0.3960 for 0% glandular, 0.3560 for 43% glandular and 0.4260 for 100% glandular, respectively [2]. Because scatter contamination in the LE and HE images can lead to erroneous calculations of the DE signals, we should estimate and correct the scatter effect. The existing methods for scatter correction in DEDM are adopting anti-scatter grids or the pinhole-array interpolation method. Although an anti-scatter grid is effective during image acquisition, it cannot completely eliminate

Medical Imaging 2009: Physics of Medical Imaging, edited by Ehsan Samei, Jiang Hsieh,
Proc. of SPIE Vol. 7258, 725840 · © 2009 SPIE
CCC code: 1605-7422/09/$18 · doi: 10.1117/12.813466

scatter effect. Problems with such a grid also include the partial absorption of primary radiation, grid line artifacts and poor efficiency with increased patient dose [3]. The pinhole-array interpolation method usually employs a lead sheet containing an array of pinholes and need extra exposures [4]. This method complicates the manipulation and is impractical for DEDM in clinic.

This paper proposed a scatter correction method for DEDM which exploits the characteristic that scatter in mammograms is a quantity of low-frequency and the fact that most pixels in mammograms are non-μCs pixels. This method only makes full use of LE and HE images, and it doesn't need anti-scatter grid, lead sheet and extra exposures. It is convenient and there is no extra dose to patients.

2. MATERIALS AND METHODS

In this paper, our investigations are based on numerical simulation. While Monte Carlo simulation (EGSnrc) [5] and Richardson-Lucy (RL) fitting acceleration [6] were used for scatter data generation, the primary data were generated by analytical computing.

The x-ray spectra were 25kVp and 50kVp with Mo anode and 0.03mm Mo filter. The spectra data were obtained from the classical Handbook [7]. The detector consisted of a CsI:Tl converter layer coupled with an aSi:H+TFT flat-panel detector. In our simulation, the scintillator thickness t_s was 45 mg/cm^2 for CsI:Tl [8]. The detector size was assumed to be 1024 x1024 pixels and each of them was 100x100μm^2. Phantoms of breast tissue-equivalent materials (Computerized Imaging Reference Systems, Inc., Norfolk, VA) with various glandular ratios were used in the calibration measurements and imaging procedures. Aluminum of different thickness was used to simulate μCs. Mass attenuation coefficients of the phantoms were calculated via the database of XCOM from NIST [9].

2.1 Calibration and inverse-mapping

A nonlinear inverse mapping technique was used to generate DE calcification images from separately acquired LE and HE images [10]. A cubic inverse mapping function could adequately model the μC thickness (t_c) as a function of the LE and HE log-signal (D_l, D_h)

$$t_c = c_0 + c_1 D_l + c_2 D_h + c_3 D_l^2 + c_4 D_h^2 + c_5 D_l D_h + c_6 D_l^3 + c_7 D_h^3 \quad , \tag{1}$$

where

$$D_l = \ln(I_{rl} / I_l), \quad D_h = \ln(I_{rh} / I_h) \quad . \tag{2}$$

I_{rj} *(j=l,h)* is the reference signal and I_j is the transmitted fluence. I_{rj} were generated through 4.5-cm-thick breast tissue-equivalent material with a glandular of 50%.The calibration data were generated with five different glandular ratios (0%, 30%, 50%, 70%, and 100%) at a fixed total tissue thickness of 4.5cm and with 6 different aluminum thickness (0, 0.038, 0.076, 0.114, 0.152, and 0.190 cm). The calibration data consisted of 30 different combinations of aluminum thicknesses and glandular ratios. The coefficients of the cubic function in Eq.(1), c_k *(k=0,...,7)*, were determined by a least-squares fit of the calibration data.

2.2 Scatter representation

The signal measured in each pixel inside the detector is the sum of the signal from the primary radiation, *P*, and that from

scattered radiation, *S*. For any pixel *i* in the LE or HE image, let

$$I_{ij}' = P_{ij} + S_{ij}, \quad j = l, h, \tag{3}$$

P_{ij} is the primary signal, S_{ij} is the scattered radiation and I_{ij}' is the measured signal. Then, D_{ij} *(j=l,h)* can be rewritten as

$$D_{il} = \ln(I_{rl}/(I_{il}' - S_{il})), \quad D_{ih} = \ln(I_{rh}/(I_{ih}' - S_{ih})). \tag{4}$$

Substituting Eq.(4) into Eq.(1), we would like to solve the scatter components S_{il} and S_{ih}. It can be seen that the coefficients c_k *(k=0,…,7)*, reference signals I_{rl} and I_{rh} , measured signals I_{il}' and I_{ih}' are all known values, and three unknowns t_{ci}, S_{il} and S_{ih} need to be solved. It is impossible to solve three unknowns using one equation. However, scatter in mammograms is a quantity of low-frequency because the breast is usually compressed to a largely uniform thickness during mammography. Therefore, the scatter of one pixel can be represented by the scatter of its neighbor pixels, polynomials and B-splines can be used to describe the relations. In this paper, the simple linear interpolation was used. For example, as illustrated in Fig.1, scatter radiation of pixel B1 can be represented as

$$S_{B1j} = (S_{A1j} + S_{A2j})/2, \quad j = l, h \quad ; \tag{5}$$

scatter radiation of pixel C1 can be represented as

$$S_{C1j} = (S_{A1j} + S_{A2j} + S_{A3j} + S_{A4j})/4, \quad j = l, h. \tag{6}$$

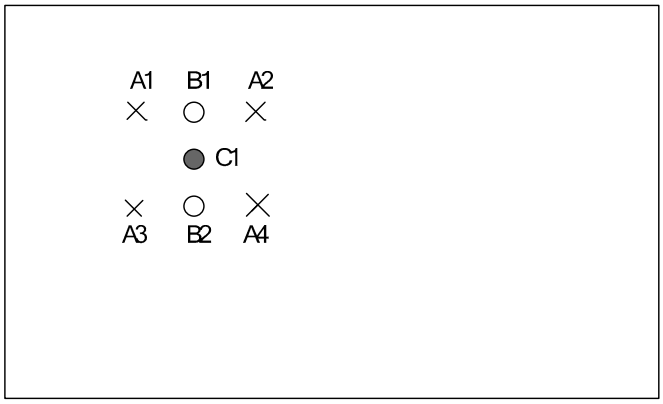

Fig.1 Sketchmap of the pixel location

2.3 Scatter estimation

For an imaged object, LE and HE images are acquired, respectively. *N* pixels in LE image and the corresponding ones in HE image can be sampled respectively. The *N* pixel pairs are put into two categories: independent pixel pairs and dependent pixel pairs. n_1 pairs are independent pixel pairs whose scatter are unknowns, as pixels Ai (i=1,2,3,4) in fig.1; n_2 ($n_2 > n_1$) pairs are dependent pixel pairs whose scatter are represented by those of independent pairs, as pixels B1,B2 and C1.

Since most pixels in mammograms are non-μCs pixels, the sample pixels can be considered as non-μCs pixels, the corresponding t_c is zero. Then, we can set up an equation set with *N* equations (Each one is Eq.(1).). There are $2n_1$ unknowns S_{ij} *(i=1,…,n1;j=l, h)* to be determined. Since N= $n_1 + n_2 > 2n_1$, the $2n_1$ unknowns S_{ij} can be determined by a least-squares fitting of the measured signals I_{ij}' *(i=1,…,N; j=l ,h)* of the *N* pixel pairs. So the scatter radiations of the n_1

pixel pairs can be obtained, scatter radiations of other pairs can be attained by interpolation. And then, the scatter distribution in the LE and HE images can be estimated.

3. RESULTS

In the experiment, the imaged object was a 4.5-cm-thick 8×4 cm^2 rectangular block of breast tissue-equivalent material with five glandular ratios 5%, 25%, 55%, 75% and 95%. For the sake of computational efficiency, the acquired LE and HE images were trimmed and only 425×841 pixels were kept. LE and HE images of the imaged object were simulated by EGSnrc and analytical computing as illustrated in Fig2. There are 307 *(N*=307*)* sample pixels in either image, including 112 *(n_1*=112*)* independent pixels (yellow) and 195 *(n_2*=195*)* dependent pixels (red and mauve) as shown in Fig2(a). Then, we had the equations set with 307 equations and 224 unknowns. A weighted least-squares fitting was employed to estimate the 224 unknowns S_{ij} *(i=1,...,112; j=l ,h)*. Since scatter radiation is a low-frequency signal, scatter radiations of other pixel pairs can be attained by interpolation. And then, the scatter distribution in the LE and HE images can be estimated.

The original scatter of any pixel *i* is S_{ij} *(j=l, h)* and the resultant scatter estimation is S_{ij}*'*. Before scatter correction, the scatter to primary ratio (SPR) is

$$SPR_{ij} = S_{ij} / P_{ij}, \quad j = l, h . \tag{7}$$

Using the proposed scatter correction method, the corrected scatter to primary ratio (SPRc) is

$$SPRc_{ij} = \left| S_{ij} - S_{ij}' \right| / P_{ij}, \quad j = l, h . \tag{8}$$

The 112 independent pixel pairs were adopted as interested pixels for comparison. Fig 3 shows the SPR and SPRc of both scatter uncorrected and corrected images. The mean, minimum, maximum and standard deviation of SPR and SPRc are listed in table 1. Fig 3 (a) and (c) show the original SPR for LE image and HE image. SPR ranges from 16.5% to 46.8% in the LE image and from 14.7% to 33.6% in the HE image without scatter correction. Fig 3 (b) and (d) show the SPRc for LE image and HE image. After scatter correction, the mean SPRc is 2.8% and the maximum SPRc is 8.8% for LE image; the mean SPRc is 0.8% and the maximum SPRc is 2.1% for HE image. It can be seen that the proposed scatter correction method works well, especially for the HE image.

The DE calcification signals of the imaged object were calculated based on the HE and LE images with and without scatter correction. Fig.4 shows the DE calcification signals of the imaged object using both scatter uncorrected and corrected images. The median, minimum, and maximum background DE calcification signals are listed in table 2. The mean background DE calcification image signal is 1678μm before scatter correction; it can be reduced to -22μm after scatter correction. The range of background DE calcification signals using scatter-uncorrected data was reduced to 2% with scatter-corrected data. So the background DE calcification signals are more accurate and the DE calculation errors introduced by scatter radiation are reduced to an acceptable level using the proposed scatter correction method. Note that the background DE calcification signals are mostly negative which means the proposed method will correct scatter radiation overly to a certain extent.

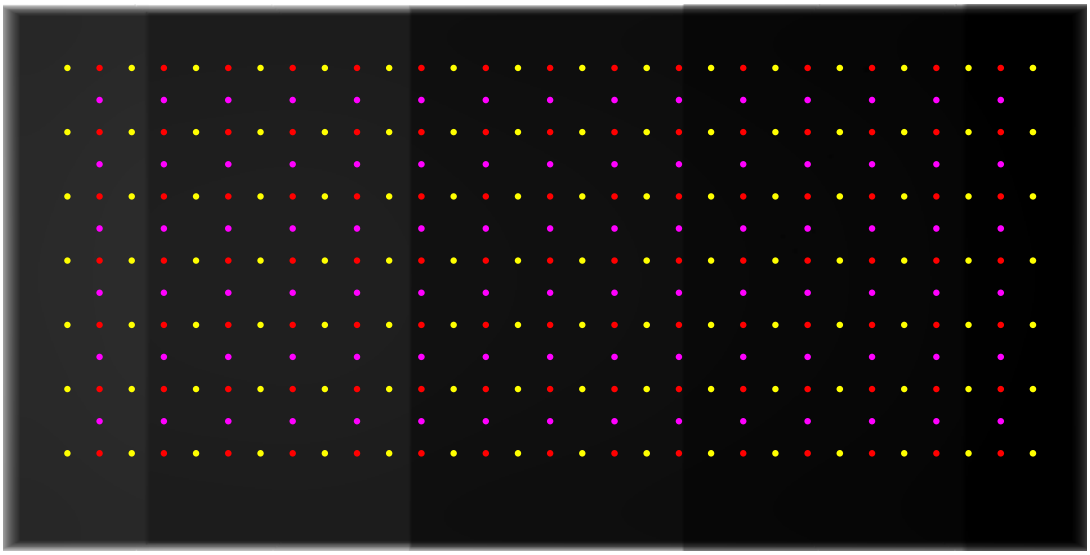

(a) LE image and the sample pixels

(b) HE Image

Fig.2 Images of the rectangular block of breast tissue-equivalent material and the positions of sample pixels.

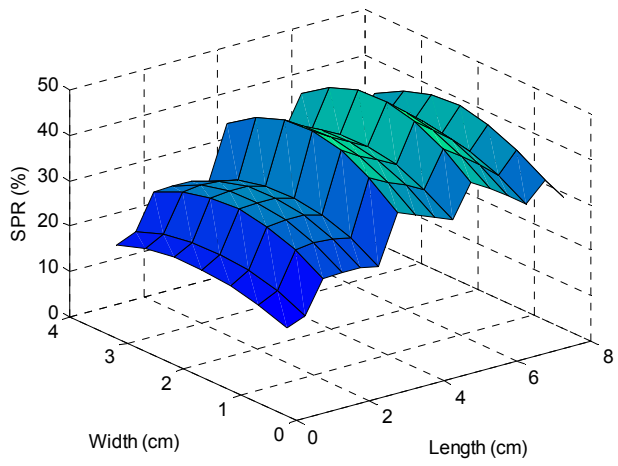

(a) SPR for LE image

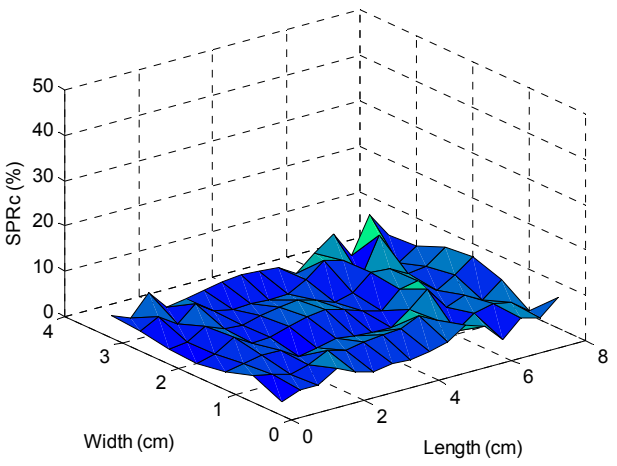

(b) SPRc for LE image

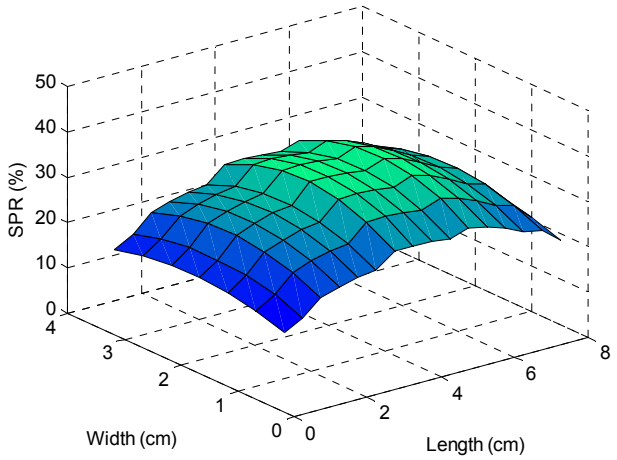

(c) SPR for HE image

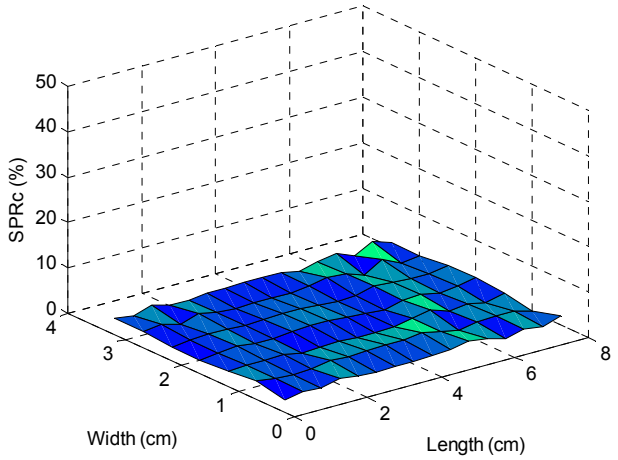

(d) SPRc for HE image

Fig.3 Scatter to primary ratio without and with scatter correction

Table 1. The mean, minimum, maximum and standard deviation of SPR and SPRc

	SPR(%)				SPRc(%)			
	Mean	Min	Max	Std	Mean	Min	Max	Std
LE	33.4	16.5	46.8	7.2	2.8	0.01	8.8	1.9
HE	26.2	14.7	33.6	4.6	0.8	0.005	2.1	0.5

Table 2. The mean, minimum, maximum and standard deviation of DE signals without and with scatter correction

Scatter Corrected	DE signals t_c (μm)			
	Mean	Min	Max	Std
No	1678	-399	3059	898
Yes	-22	-59	18	14

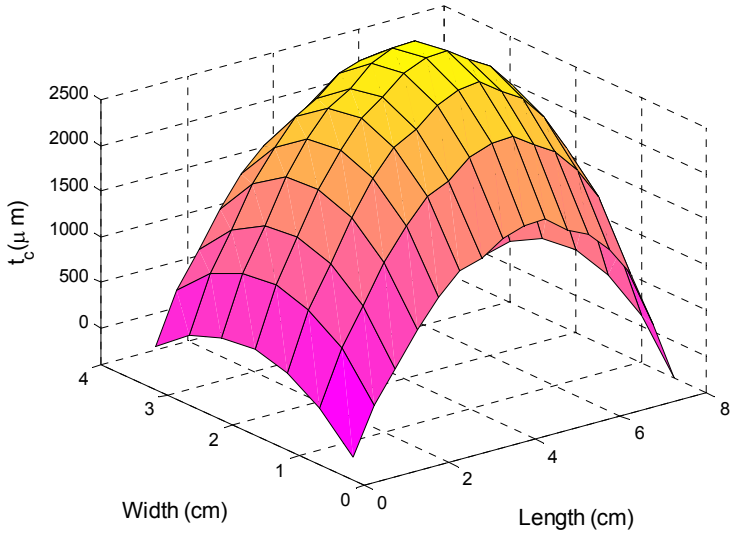

(a) scatter-uncorrected

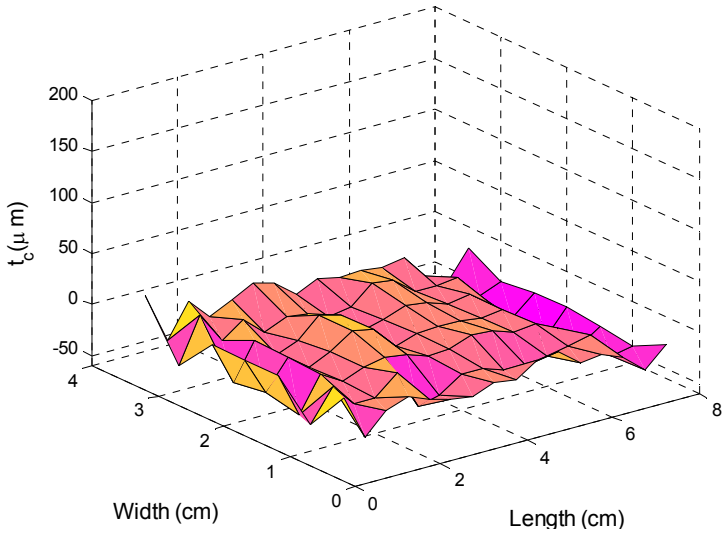

(b) scatter-corrected

Fig.4. Background signal of the DE calcification images of the imaged object using scatter-uncorrected and scatter-corrected images.

4. CONCLUSION

A scatter correction algorithm for DEDM is developed based on the fact that scatter in mammograms is a quantity of low-frequency and most pixels in mammograms are non-μCs pixels. The method only uses the information of LE and HE images and it doesn't need anti-scatter grid, lead sheet and extra exposures. It is convenient and there is no extra dose

to patients. The results show that the scatter correction method is effective. When using the simple least-squares fit and linear interpolation, SPR can be decreased to 2.8% for LE image and 0.8% for HE image. When applying the scatter correction to LE and HE images, the resultant background signal in the DE calcification image can be significantly reduced. Using the scatter correction method will make the DE calculation more accurate.

ACKNOWLEDGEMENTS

The project is partially supported by the National Science Fund of China (No. 60472004 and No. 60551003), the fund of the Ministry of Education of China (No. 106143), and the fund of ICRG of Hong Kong Polytechnic University (YG-79).

REFERENCES

[1] American Cancer Society, "Breast Cancer Facts & Figures 2005-2006*"*. Atlanta: American Cancer Society. INC (2005).

[2] Cooper III, Virgil N., Boone, John M., Seibert, J. Anthony and Pellot-Barakat, Claire J., "An edge spread technique for measurement of the scatter-to-primary ratio in mammography," Med.Phys.27, 845–853(2000).

[3] Nykänena, Kirsi and Siltanen, Samuli, "X-ray scattering in full-field digital mammography," Med.Phys.30, 1864–1873 (2003).

[4] Kappadath, S. C. and Shaw, C. C., "Dual-energy digital mammography for calcification imaging: scatter and nonuniformity corrections," Med.Phys. 32, 3395–3408(2005).

[5] Kawrakow, I. and Rogers, D. W. O., "The EGSnrc Code System: Monte Carlo Simulation of Electron and Photon Transport, NRCC Report PIRS-701." http://www.irs.inms.nrc.ca/EGSnrc/pirs701/index.html (2007).

[6] Colijn, A. P. and Beekman, F. J., "Accelerated Simulation of Cone Beam X-Ray Scatter Projections," IEEE Trans on Med. Imaging, 23, 584-590 (2004).

[7] Fewell, T. R. and Shuping, R. E., [Handbook of Mammographic X-ray Spectra], Rockville, MD: Bureau of Radiological Health, 25–70 (1978).

[8] Lemacks, M. R., Kappadath, S. C., Shaw, C. C., Liu X. and Whitman, G. J., "A dual-energy technique for microcalcification imaging in digital mammography: a signal-to-noise analysis," Med. Phys. 29, 1739–1951 (2002).

[9] Berger, M. J., Hubbell, J. H., Seltzer, S. M., Chang, J., Coursey, J. S., Sukumar R. and Zucker, D. S., "XCOM: Photon Cross Section Database (version 1.3). http://physics.nist.gov/xcom," National Institute of Standards and Technology, Gaithersburg, MD. (2005).

[10] Kappadath, S. C. and Shaw, C. C., "Dual-energy digital mammography: calibration and inverse-mapping techniques to estimate calcification thickness and glandular-tissue ratio," Med. Phys. 30, 1110–1117 (2002).